Ecological Informatics 85 (2025) 102947

Contents lists available at ScienceDirect

Ecological Informatics

journal homepage: www.elsevier.com/locate/ecolinf

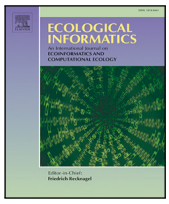

An auto-tuning process-based 3D model to forecast irrigation demand in kiwifruit

Marco Bittelli [a], Matteo Francia [b], Joseph Giovanelli [b], Matteo Golfarelli [b,*], Fausto Tomei [c]

[a] Department of Agricultural and Food Sciences, University of Bologna, Italy
[b] Department of Computer Science and Engineering, University of Bologna, Italy
[c] Regional Agency for Prevention, Environment and Energy, Emilia Romagna, Italy

ARTICLE INFO

Dataset link: https://github.com/big-unibo/orchard3d-lab, https://big.csr.unibo.it/projects/orchard3d-lab

Keywords:
Irrigation demand forecasting
State initialization
Root system
Kiwifruit
3D process-based model
Bayesian parameter tuning procedure

ABSTRACT

In a contest of climate change and increasing world population, the optimization of agricultural inputs such as water and fertilizer is of utmost importance to assure crop quality and to limit the impact of agriculture. For these reasons, the need for robust methods of agricultural modeling and forecasting has never been clearer. In particular, forecasting the water budget is a key tool for reducing water wastage and maximizing agricultural production. Although process-based models are largely used in off-line simulation and studies, their operational use in forecasting the irrigation requirements of a specific crop remains complex and the level of accuracy achieved is often insufficient since, if used alone, process-based simulation systems fail to capture the soil and plant dynamic behaviors. To overcome these limitations we propose an integrated system coupling Orchard3D-Lab, an innovative three-dimensional process-based model specifically devised for fruit trees, with a state initialization procedure that exploits a two-dimensional probe grid. The system is capable of auto-tuning its parameters on a specific soil and of providing a precise forecast that can support precision watering policies on a weekly horizon. A large set of tests has been conducted on Kiwifruit in an experimental farm in Northern Italy. Besides accuracy, tests proved the robustness of the system even in the presence of a limited set of examples for parameter auto-tuning. This makes our approach concretely applicable in real-world settings.

1. Introduction

The possibility to accurately and precisely forecast agricultural systems can provide significant improvement in many agricultural issues such as irrigation demand, drought, climate change, nutrient depletion, and soil degradation (Lv et al., 2021). Forecasts can be obtained by running a simulation model for a specific environment. The forecast accuracy is directly related to the type of application. Forecasting the water budget in a prescriptive irrigation system is among the most challenging applications since the decision to irrigate or not to irrigate requires high accuracy. In Silva and Giller (2020), the authors presented a series of relevant doubts regarding the ability of pure process-based[1] crop models to precisely forecast water budget at the operational level. The uncertainty associated with process-based crop models can be reduced by coupling such models with real-time acquisition of relevant soil and crop variables (Ye et al., 2014). Today, with digitalization and remote acquisition of real-time data it is possible to effectively incorporate experimental data and carry out simulations in real-time (Vitali et al., 2021).

Fruit trees are still under-represented in crop models. Their extensive leaf area, which varies dynamically throughout the season, and root system must be explicitly taken into account for accurately simulating soil moisture. Our study focuses on the kiwifruit (*actinidia deliciosa*), often shortened to kiwi (used hereafter): an edible fruit characterized by a high water demand (Judd et al., 1986). In Italy, the third largest producer worldwide, kiwi uses every year about 5000 to 6000 cubic meters of water per hectare (Judd et al., 1986) throughout the whole season. In the Emilia-Romagna region (Italy), the kiwi irrigation season generally starts in May and ends in October (Villani et al., 2011), therefore with high water demands in a period where droughts and water scarcity are becoming more frequent due to climate change.

* Corresponding author.
E-mail addresses: marco.bittelli@unibo.it (M. Bittelli), m.francia@unibo.it (M. Francia), j.giovanelli@unibo.it (J. Giovanelli), matteo.golfarelli@unibo.it (M. Golfarelli), ftomei@arpae.it (F. Tomei).

[1] A process-based model is the mathematical representation of a physical process characterizing the functioning of a well-delimited biological system. Usually, such models consist of a set of ordinary or partial differential equations that define the essence of each process, as well as their inputs and outputs.

https://doi.org/10.1016/j.ecoinf.2024.102947
Received 23 July 2024; Received in revised form 5 December 2024; Accepted 6 December 2024
Available online 13 December 2024

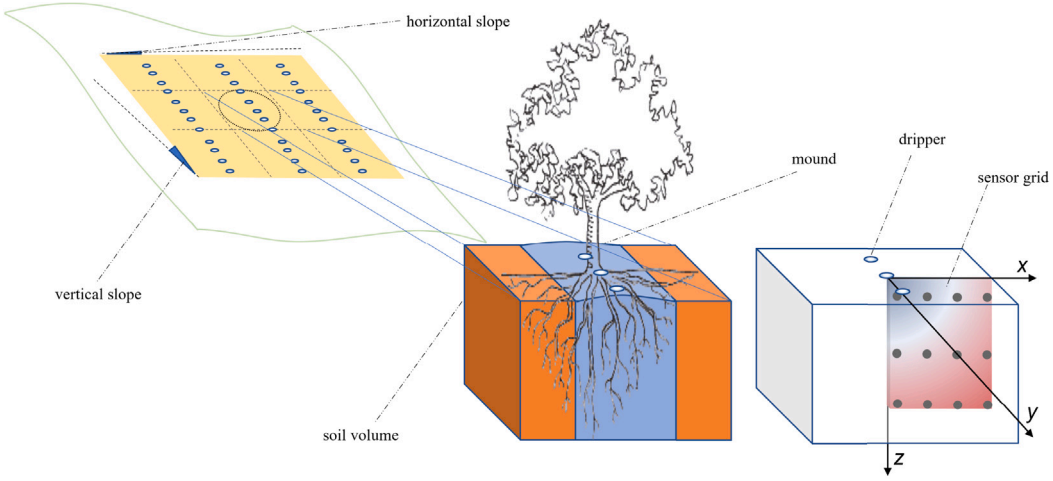

Fig. 1. Schematic depicting the planting layout.

Few research papers have been published on measuring and modeling kiwi water demand. Indeed, in a review on fruit tree crop models, Grisafi et al. (2022) showed that only one research was published on modeling kiwi, but the emphasis was on the carbon budget and not on the soil water budget. Little has also been done in terms of modeling the plant's water use and transpiration. Rallo et al. (2021) presented a review of FAO56 crop coefficients of fruit trees and vines, performed over the past twenty years, to update information and extend tabulated single and basal standard crop coefficients. Also in this review, it appears that kiwi is highly under-represented with only one listed research by Silva et al. (2008), where kiwi's transpiration was measured with a sap flow method.

At the heart of a soil moisture forecasting system there is a robust water budget simulation model capable of computing the Soil Water Content (SWC) and Soil Water Potential (SWP) in the root zone and providing the right water amount to keep the cultivated plant in optimal conditions. A water budget model implies the measurement and/or the computation of a variety of soil processes including surface runoff, deep percolation into the groundwater, capillary rise from the groundwater, subsurface lateral flow, soil evaporation, and plant transpiration (Marshall et al., 1996). Most of the previous process-based models in the literature (e.g., DSSAT (Sau et al., 2004), APSIM (Keating et al., 2003)) are far from modeling these soil processes at the required precision level, and none of them are specialized in key factors of fruit trees such as root architecture. Forecasting the water balance is also useful in many other soil-related applications. For example, Bioclim (Serrano-Notivoli et al., 2022) is a software for bioclimatic classification that computes the water balance at a very coarse grain (i.e., month and region). Even having a specialized model at hand, making it operational in a real-world context requires solving two complex problems: (1) how to choose model parameters to simulate a specific field; and (2) how to handle the inevitable model drifts.

In the majority of papers, the parameters of process-based simulation models are obtained by off-line measures carried out in laboratories. However, these measurements are expensive, time consuming, and rarely a feasible solution for farmers in an operational setting. An alternative solution is to install soil probes measuring SWC or SWP and calibrate the model through a parameter tuning procedure that progressively aligns the simulation model to the measured data. Obviously, given the huge size of the parameter space, it is hard to optimize such alignment so that the simulation model can run even with a limited set of real data.

In real-case problems, there are no error-free estimations. Many slight errors gradually accumulate and lead the model to progressively diverge from the expected behavior, especially for domains in which many phenomena interact and influence each other. In particular, soil moisture is affected by weather forecasts, water tables, soil slopes, hysteresis, and so on. In these cases, the availability of real measurements sampled by the probes can be used to initialize the state of the simulation model, reset the drift, and set the error level to zero. The uncertainty on the soil moisture value will increase for the portions of the soil volume that are farther from the probe. In our approach, we exploit an innovative grid of probes (Baldi et al., 2023) rather than a single one. This makes it possible to create a precise map of the water content that, in turn, makes the model initialization a powerful tool. Today many companies commercialize affordable and reliable probes installable in orchards (Bittelli, 2010; Nagahage et al., 2019).

Summing up, in this paper we propose:

- Orchard3D-Lab, an innovative *3D process-based model* specifically devised to compute the soil water balance of an orchard. The 3D model takes into account the non-uniform distribution of the root system and the growth and development of orchard plants with a full computation of the soil water budget.
- A *Parameter Tuning* technique to automatically calibrate the model parameters to a specific orchard through a Bayesian hyper-parameter tuning procedure.
- A *State Initialization* technique to map coarse-grained 2D/3D-probe grid to the fine-grained 3D state of Orchard3D-Lab.
- A detailed field experiment in a commercial Kiwifruit orchard.

2. System design and techniques

Fig. 1 depicts the planting layout adopted in this paper. Trees are arranged in lines and soil can have a slope both in the x and y axes. The orchard is equipped with a watering system of different types (e.g., single or double wing) and different distances between drippers and lines. For each plant, we consider a *soil volume* that includes the roots; typically the soil volume can be larger than the area affected by the watering system. A mound can be present to favor draining.

The simulation approach and the required functional modules are depicted in Fig. 2. The offline phase determines the optimal process-based model parameters. The *Parameter Tuner* searches for the best parameters by comparing data simulated by the process-based model named Orchard3D-Lab with the *Historical Data* from real probes. Historical data must cover the period of the simulation scenario, including watering and weather conditions (typically obtained from in-situ weather stations or public open data) together with their effect on soil water content (i.e., the values sampled by soil probes).

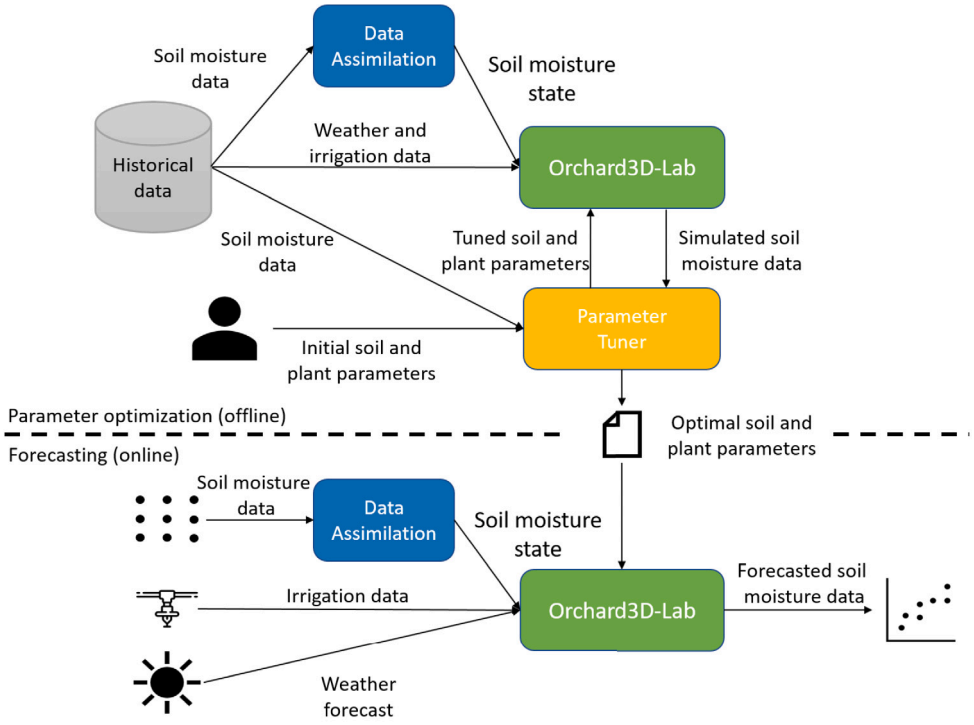

Fig. 2. Approach overview and main system components.

The online phase requires the grid of probes to be in place. During this phase Orchard3D-Lab, properly set with the optimal parameters, forecasts the system behavior and exploits *State Initialization* to initialize the simulation model to the real field status.

Table 1 shows the simulation parameters: in bold those automatically inferable by the tuning phase, while the remaining ones must be provided by the user. Note that if no historical values are available, tuning cannot be run. In this case, the online phase will be based on default values possibly taken from the literature. Similarly, if some of the tunable parameters are known, tuning can be limited to the remaining ones.

The following subsections describe in more details the components reported in Fig. 2.

2.1. Orchard3D-Lab: the orchard simulation model

We present an innovative process-based simulation model specifically devised for computing the soil water budget in an orchard. The numerical solution is based on the integrated finite difference (also called cell-centered finite volume scheme) method. Orchard3D-Lab builds on Criteria-3D (Bittelli et al., 2015) and introduces the following innovative features in the computation of the soil water budget in an orchard:

- a dynamic model for evapotranspiration that keeps into account plant growth along the season (see Section 2.1.2);
- an advanced root's system model that models variable root density (see Section 2.1.3);
- application of the three-dimensional computation specifically for an orchard with land slopes and drip irrigation system; and
- state initialization from a probe grid.

Orchard3D-Lab accounts for saturated water flow, unsaturated water flow, and surface runoff. It is also coupled with a model for soil evaporation and plant water uptake. The soil moisture state, at a certain time t, is stored as a 3D matrix (SM_t) where each cell represents a portion of the soil volume along with its simulated soil moisture.

The modeling approach in Orchard3D-Lab is comparable to other process-based models that solve the governing equation of water flow with numerical methods, such as Hydrus-3D (Honari et al., 2017) that was also applied in orchards (Morianou et al., 2023). However, our model has a novel and detailed characterization of spatial and temporal root growth and development, as detailed in the following sections of the manuscript.

Algorithm 1 describes how a simulation is computed. Starting from a state initialized with probe data, an iterative process computes soil moisture given the time series of weather and irrigation data. More in detail, Orchard3D-Lab takes as inputs the probe values at the initial timestamp (S_{t_0}), a time series of weather forecasts at increasing timestamps ($\overline{W}$= [(t, humidity, air temperature, solar radiation, wind speed), …]), a time series of irrigation at increasing timestamps ($\overline{I}$= [(t, irrigation), …]), and the set of parameters X from Table 1. We assume $\overline{W}$ and $\overline{I}$ to be aligned over time and to be at the same time granularity of the simulation. First, we initialize the simulator state (as described in Section 2.2) with the probe data mapped to the simulator fine-grained 3D matrix (Line 1) and the time series in which the simulated soil moisture will be accumulated (Line 2). For each timestamp (Line 3), the current weather, irrigation, and simulator state are leveraged to update the state of the simulator using the Richards equation (Line 4), the new state is accumulated (Line 5) and updated (Line 6). Finally, the time series of soil moisture over the whole period is returned (Line 7).

Orchard3D-Lab solves Richards' equation (Richards, 1931) to compute water flow. For each cell of soil in our 3D matrix, it calculates the change of the water potential and volumetric water content in time. This demands information about (i) the soil hydraulic properties, (ii) the amount of water to sink (e.g., for the root water uptake), and (iii) the boundary conditions (i.e., behavior at the boundary of the soil volume at hand). In the following, Section 2.1.1 provides the main

Table 1
System parameters.

Type	Parameter	Description
Field	Location	Latitude, longitude and altitude [m] of the field
	Slopes	Slopes [$m \cdot m^{-1}$] of the simulated field
	Mound	Slope [$m \cdot m^{-1}$] and width [m] of the mound
	Water table $\in$ [1.5..5]	Depth [m] of a aquifer
Soil Layer[a]	Thickness	Thickness [m] of the soil layer moved from Domain
	Texture	Portion of sand, silt and clay [%]
	Ksat $\in [10^{-7}..10^{-3}]$	Saturated hydraulic conductivity
	$\boldsymbol{\theta_s} \in$ [0.2..0.7]	Saturated water content [−]
	$\boldsymbol{\theta_r} \in$ [0.02..0.7]	Residual water content [−]
	$\boldsymbol{\alpha} \in$ [0.5..5]	Modified Van Genuchten inverse air entry suction [m^{-1}]
	n $\in$ [1..2]	Modified Van Genuchten pore-size distribution
	he $\in$ [0..15]	Modified VanGenuchten/Campbell air mat. pot. [mH_2O]
	b $\in$ [1..9]	Campbell empirical retention parameter
Plant[a]	Position	Position [m] of the plant (s) in the domain area
	Radius $\in$ [1..3]	Radius [m] of the canopy
	Leaf area index $\in$ [3..5]	Green leaf area per unit ground surface area
	Roots depth $\in$ [0.5..1.2]	Origin and maximum depth [m] of roots
	Roots deformations $\in$ [0..2]	Root deformation factors on x and z axes
	Kc max $\in$ [0.8..4]	Maximum crop coefficient
	fRAW $\in$ [0..1]	Readily available water fraction
Irrigation elem[a]	Type	Irrigation type of the element (s)
	Position	Position of the element (s)
Model	Geometry	Length × Width × Depth [m] of the simulated field
	Cell size	Size [m] of a single parallelepipeds simulation unit
	Ret. curve $\in$ [*Camp.*, *modVanGenuc.*]	Water retention model
	Conduct. mean $\in$ [*log*, *harm*, *geom*]	Water conductivity averaging method
	Conductivity H/V Ratio $\in$ [0..1]	Water conductivity horizontal/vertical ratio

Parameters in bold are targeted by the parameter tuning.
[a] Types can have several elements.

Algorithm 1 Orchard3D-Lab

Require: S_{t_0}: Probe-level moisture state, $\overrightarrow{W}$: weather time series, $\vec{I}$: irrigation time series, X: parameters from Table 1
Ensure: $\overrightarrow{SM}$: time series of simulated soil moisture
1: $ST \leftarrow$ StateInitialization(S_{t_0}) ▷ Map probe data to the initial state
2: $\overrightarrow{SM} \leftarrow [\,]$ ▷ Initialize the accumulator
3: **for each** $t \in \overrightarrow{W}, \vec{I}$ **do** ▷ For each timestamp…
4: $ST_{new} \leftarrow Richards(ST, w_t, i_t, X)$ ▷ … calculate the next state
5: $\overrightarrow{SM} \leftarrow \overrightarrow{SM} \frown (t+1, ST_{new})$ ▷ … append it
6: $ST \leftarrow ST_{new}$ ▷ … update it
7: **return** $\overrightarrow{SM}$ ▷ Return the time series of soil moisture

equations leveraged by Orchard3D-Lab to estimate the soil hydraulic properties; Sections 2.1.2 and 2.1.3 describe how to obtain the root water uptake for each portion of soil by, respectively, calculating the overall volume of water leaked for transpiration and splitting it according to the root system; finally, Section 2.1.4 delves into the boundary conditions.

2.1.1. Soil hydraulic properties

Richards' equation is the solution of the mass balance for water in a soil volume. A fundamental component in its resolution is the description of the hydraulic properties, namely the soil water retention and the hydraulic conductivity function.

The soil water retention curve maps the soil water potential (i.e., the driving force for flow) to the soil water content (i.e., the amount of water) and is used to describe the drying process of a particular soil. For its estimation, the van Genuchten–Mualem model is currently the most widely exploited. Yet, it has been demonstrated that it can lead to erroneous estimates of hydraulic conductivity. For this reason Orchard3D-Lab employs the modified van Genuchten–Mualem model proposed in Ippisch et al. (2006), where an air entry value is included in the formulation:

$$S_e(h) = \begin{cases} \frac{1}{S_c}\left[1 + (\alpha h)^n\right]^{-m} & \text{if } (h > h_e) \\ 1 & \text{if } (h \le h_e) \end{cases} \quad (1)$$

Given the inverse air entry suction α (i.e., the value for which we mark the transition between saturated and unsaturated soil mechanics), $m = 1 - \frac{1}{n}$ a shape-defining pore parameter derived from the pore-size distribution (depending on soil texture and structure), and $S_c = [1+(\alpha h_e)^n]^{-m}$ the water saturation at h_e the air-entry potential (i.e., the point at the largest pores which air can enter into the soil); the degree of saturation S_e is defined in relation to the soil water potential h.

Hydraulic conductivity is the ease with which water moves through porous spaces and fractures in soil (e.g., porous soil has a high hydraulic conductivity if water can readily travel through it). In other words, the flux density is regulated by the ability of the material to transfer water under a certain gradient. Given a "tortuosity" factor l, it is possible to calculate the hydraulic conductivity K in relation to the current degree of saturation S_e as:

$$K(S_e) = \begin{cases} K_s S_e^l \left[\frac{1-(1-(S_e S_c)^{\frac{1}{m}})^m}{1-(1-S_c^{\frac{1}{m}})^m}\right]^2 & \text{if } (S_e < 1) \\ K_s & \text{if } (S_e \ge 1) \end{cases} \quad (2)$$

The parameter K_s is the saturated hydraulic conductivity, which represents the ability of the soil to conduct water when all the pores are water-filled. When the soil starts to desaturate (drying), the hydraulic conductivity decreases with respect to its value at saturation. The parameters m and n allow the curve to take different slopes and shapes in decreasing values from saturation, again depending on texture and structure.

2.1.2. Evaporation and plant growth-aware transpiration

Leaf growth in fruit trees causes transpiration to vary greatly throughout the season. For proper modeling of the phenomenon, it is necessary to model this dynamicity.

The classic approach to estimating the amount of water transpired by the plant is to compute the overall potential evapotranspiration and, then, calculate the plant's transpiration based on the plant's vigor. The potential evapotranspiration ET_0 is calculated by the Penman-Monteith equation for the typical reference crop (Allen et al., 1998). Given the fraction of intercepted Photosynthetically Active Radiation $fPAR$, and the momentary Turbulence Coefficient TC, we can derive (under optimal conditions) the maximum potential transpiration T_{pot} and evaporation E_{pot}:

$$T_{pot} = ET_0 \cdot fPAR \cdot TC \tag{3}$$

$$E_{pot} = ET_0 \cdot (1 - fPAR) \tag{4}$$

The fraction of absorbed photosynthetically active radiation $fPAR$ is defined in relation to the Leaf Area Index LAI (i.e., the quantity of unilateral green leaves per square inch of soil that estimates the plant canopy growth) through the light extinction coefficient KE, set at the average value of 0.6. In turn, LAI varies throughout the year according to the plant vigor; to model such dynamicity we leverage on SDD (i.e., Sum of Day Degrees accumulated by the plant during the growing season):

$$fPAR(SDD) = 1 - e^{-KE \cdot LAI(SDD)} \tag{5}$$

$$LAI(SDD) = \frac{LAI_{max} - LAI_{min}}{1 + e^{(a_{LAI} + b_{LAI} \cdot SDD)}} + LAI_{min} \tag{6}$$

LAI_{max} and LAI_{min} are the maximum and minimum LAI values respectively, while a_{LAI} and b_{LAI} are crop dependent parameters. Such LAI parameters can be found in literature, and hence derive its value only from SDD.

Finally, the turbulence coefficient TC depends on the crop coefficient $Kc(SDD)$, a fraction of the water needed for the reference high-water-use grass crop. Specifically, TC is the crop coefficient for the mid-season development stage of adequately watered crops (Driessen and Konijn, 1992):

$$TC(SDD) = 1 + (Kc_{Max} - 1) \cdot fPAR(SDD) \tag{7}$$

Kc_{Max} is the value of the crop coefficient when the plant has the maximum value of LAI (Allen et al., 1998). Its value is either obtained from the literature or calibration.

2.1.3. Root system

Fruit trees have a significant root system whose shape, extension, and density must be considered to properly model soil volume moisture. In Orchard3D-Lab, the overall potential transpiration T_{pot} is divided among each portion of the soil that contains the root system. The root uptake in a specific point $actTrans(x, y, z)$ varies according to the respective root density $k_{root}(x, y, z)$. The greater the density, the greater the portion of T_{pot} that is transpired in that point:

$$actTrans(x, y, z) = T_{pot} \cdot k_{root}(x, y, z) \tag{8}$$

By default, the root shape is the "taproot". Besides being a common tree crop, this is generally assumed in kiwi trees. This is customizable according to the following conditions:

- along the x axis, the root density varies linearly w.r.t. the distance to the dripper line, a parameter (i.e., $root_x$) allows to set a constant density or to drop it to zero at the inter-row;
- along the y axis, the root density is assumed to be constant, this is consistent with the model assumptions of constant water content along the dripper line;
- along the z axis, the root density is non-linear, a parameter (i.e., $root_z$) allows to set higher density either in the upper or lower layers.

The values of $root_x$ and $root_z$ can be deduced by the Parameter Tuner.

Fig. 3 shows the root density projections on the xy and xz planes. The parameter values shaping the figure routes are those set in the orchard adopted in our experimentation. Note how moving further away from the center, where the dripper is located, root density decreases both vertically and horizontally.

2.1.4. Boundary conditions

To numerically solve the partial differential equations governing Richards water flow, boundary conditions are used to reduce the number of unknown variables. In practice, we define the behavior of the soil at the boundaries of the simulated volume so that we can determine the solution of the equation (i.e., the value of the flux) in the part of interest. To properly solve the problem, the boundary conditions should represent the actual conditions of the experiment and, hence, be chosen upon the available information (in this regard, details can be found in Bittelli et al. (2015)).

Orchard3D-Lab allows to set up Dirichlet and Neumann boundary conditions. The former defines the specific value the flux needs to take along the boundary, the latter defines the desired derivative. As to Dirichlet boundary conditions, we implemented: nodes (i.e., portions of soils) with fixed hydraulic head (i.e., fixed water potential), and nodes with prescribed flux (i.e., fixed source/sink phenomena). The water table is a simple example of nodes with fixed hydraulic heads; when this is present, the water potential is set to zero at the water table depth. Atmospheric boundary conditions are examples of nodes with prescribed flux. Positive fluxes are assigned to the surface for either precipitation or irrigation events, and negative fluxes to the upper soil layers and rooting depth for potential evapotranspiration. As to Neumann boundary conditions, the model implements free drainage at the boundaries as a bottom outflow. The gradient is determined based on the elevation difference among computational nodes, with the first node in a position outside the computational domain.

2.2. State initialization

The state initialization process maps in-situ probe data to a state of Orchard3D-Lab. This is used as the initial state of Orchard3D-Lab, in this way the forecast begins from an actual soil condition (Fig. 4(a)). Of course, the more the probes (e.g., gypsum-blocks; Fig. 4(b)), the better the granularity of the sampling and the accuracy of the initial state. Such accuracy also depends on the probe layout: the higher the dimensionality of the layout, the fewer the assumptions to be made:

- most of the approaches in the literature rely on a single probe and assume the soil moisture to be constant over the whole soil volume;
- a one-dimensional (1D) grid relies on a column/row of probes and assumes the soil moisture to be constant over horizontal/vertical planes;
- a two-dimensional (2D; Fig. 4(b)) grid relies on a 2D matrix of probes and assumes the soil moisture to be constant over adjacent slices;
- a three-dimensional (3D) grid measures soil moisture as is and makes no symmetry assumptions.

Orchard3D-Lab simulations are carried out on a fine-grained 3D grid, where the size of a single cell is 1 cm. Since it is not feasible to have a real probe in each cell, the soil moisture for the virtual fine-grained grid must be estimated starting from the coarse-grained grid of real probes. In Francia et al. (2022), we introduced several *profiling functions* that approximate the soil moisture sampled by a coarse-grained 2D/3D probe grid to a *refined grid* with finer granularity (Fig. 4(c)). For the sake of conciseness, we describe the linear profiling function in a 2D scenario. Given a 2D probe grid, the profiling function

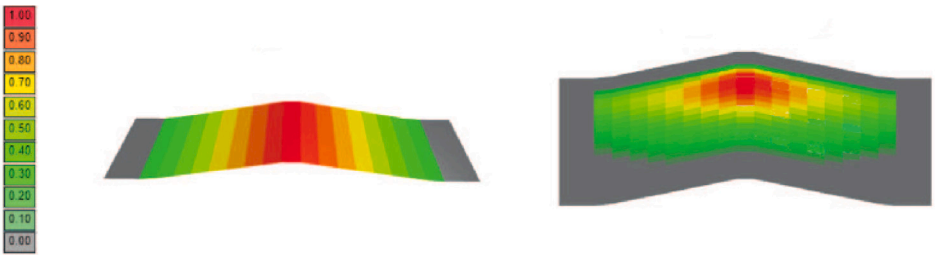

Fig. 3. Root schematic: variation of the root density on the xy plane (on the left) and on the xz plane (on the right).

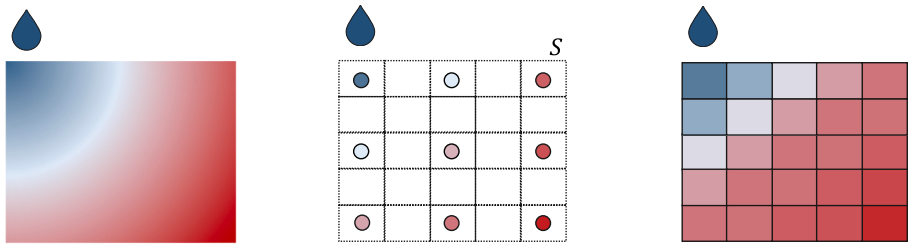

(a) Actual soil moisture. (b) Raw probe grid (c) Soil profile

Fig. 4. Snapshot of soil moisture in a soil slice; the water drop represents a dripper.

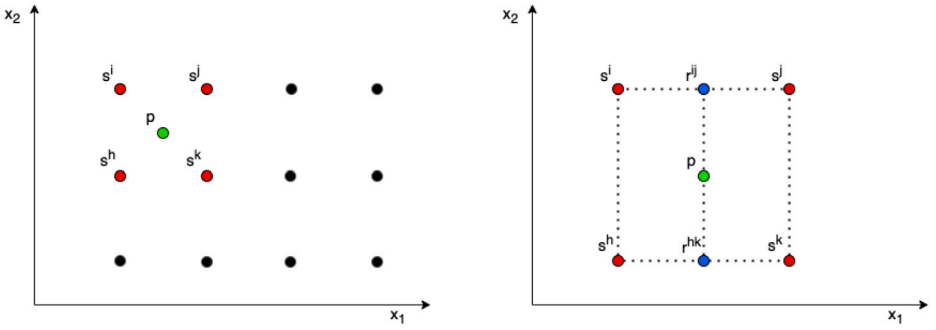

(a) Bounding rectangle: in green the point to be approximated, in red the probes enclosing it. (b) Bilinear interpolation: blue values rs are interpolated first, then p.

Fig. 5. A 2D example of the profiling function.

carries out a bi-linear interpolation of soil moisture. The approach consists of two phases (Fig. 5). For each point to be calculated: (i) we find the four probes that determine the minimum bounding rectangle enclosing it (Fig. 5(a)); then (ii) we interpolate along the first axis obtaining the moisture values on intermediate points and we determine the desired value by interpolating the intermediate values along the second axis (Fig. 5(b)).

To ensure precise sensing, we consider 2D and 3D probe grids since they rely on fewer symmetry assumptions. Symmetry assumptions also depend on the dripper layout. In this work, we refer to a single-line dripper watering system (Fig. 6) where the probe grid is orthogonal to the dripper line (Fig. 4(b)). The $StateInitialization$ function relies on the profiling function to obtain a refined grid from a probe grid (Fig. 4(c)), then it applies the necessary geometric transformations to complete the whole soil volume (i.e., the simulator state):

- given a 2D refined grid, the (3D) soil moisture state SM_t is obtained by translating the refined grid along y axis and by reflection on the x axis (Fig. 6);
- given a 3D refined grid, the (3D) soil moisture state SM_t is obtained by reflection one the x axis.

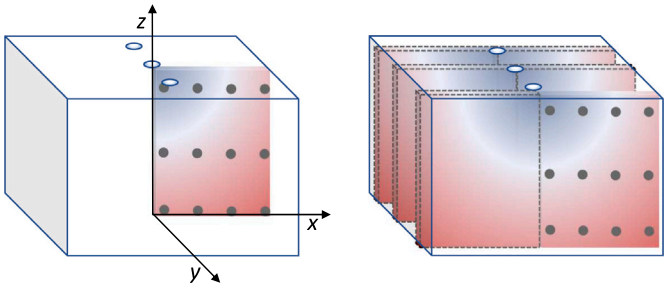

Fig. 6. Transforming a 2D probe grid (left) into a state of Orchard3D-Lab (right) through translation and reflection geometric transformations.

2.3. Parameter tuner

Due to the huge number of parameters (Table 1), manual or brute-force tuning of Orchard3D-Lab is unfeasible. Our Parameter Tuner automatically calibrates the model parameters to fit a specific orchard behavior as described by probe data. In the literature, there are numerous optimization methods to find the best configuration

Algorithm 2 Parameter Tuner

Require: $\overrightarrow{W}$: weather time series, $\overrightarrow{I}$: irrigation time series, X_{fix}: fixed parameters, $budget$: maximum iterations, $\overrightarrow{S}$: probe soil-moisture time series
Ensure: X_{tun}: best parameter configuration

1: $H \leftarrow \varnothing$ ▷ History of explored configurations
2: $iteration \leftarrow 0$ ▷ Current iterations
3: **while** $iteration < budget$ **do** ▷ While some budget remains
4: $iteration \leftarrow iteration + 1$ ▷ … increase the iterations
5: $X_{tun} \leftarrow BayesianOpt(H)$ ▷ … optimize the "free" parameters
6: $\overrightarrow{SM} \leftarrow$ Orchard3D-Lab$(S_{t_0}, \overrightarrow{W}, \overrightarrow{I}, X_{tun} \cup X_{fix})$ ▷ … run the simulator
7: $e \leftarrow error(\overrightarrow{SM}, \overrightarrow{S})$ ▷ … get the error
8: $H \leftarrow H \cup \{(X_{tun}, e)\}$ ▷ … add the configuration to the history
9: Return $\underset{X_{tun}\ s.t.\ (X_{tun},e)\in H}{\operatorname{argmin}} e$ ▷ Return the best configuration

over huge search spaces (Luo et al., 2017). Since exhaustive search is unfeasible, these methods operate under a budget in terms of execution time or configurations to visit. First, they evaluate the performance of an initial (possibly random) configuration. Then, they converge to better configurations by selectively exploring only a portion of the search space. We employ Bayesian Optimization (BO) (Frazier, 2018), which constructs a surrogate model of the search space to identify the most promising regions. We incorporate priors in the definition of the search space through parameter distributions, such as log-scales or agronomist-derived default values. While exploring configurations, BO balances exploitation (seeking high predicted performance) and exploration (seeking configurations with higher uncertainty), thus updating the surrogate model as more configurations are explored. BO returns the best configuration after the exploration budget is exhausted, alongside uncertainty estimates for each parameter. To enhance this process, we utilize the Blended-search approach (Wang et al., 2021) from the FLAML package, which augments standard Bayesian Optimization with local search capabilities. This hybrid approach focuses additional exploration on regions with promising configurations while minimizing computational costs associated with evaluating poor configurations, thus addressing challenges related to parameter identifiability.

The Parameter Tuner is detailed in Algorithm 2 and takes as inputs: weather and irrigation time series, the soil moisture time series sampled by probes (our ground truth), a maximum iteration budget, and the subsets of (manually) fixed and automatically-tunable parameters ($X_{fix} \cup X_{tun} = X$ and, $X_{fix} \cap X_{tun} = \varnothing$, with X being the parameters from Table 1). Algorithm 2 returns as output the configuration of parameters that allow Orchard3D-Lab to produce the best approximation of real probe values (i.e., of our ground truth). Given the simulation states $\overrightarrow{SM}$ and the sampled soil moisture $\overrightarrow{S}$, the error of approximating $\overrightarrow{S}$ with $\overrightarrow{SM}$ is computed as follows

$$error(\overrightarrow{SM}, \overrightarrow{S}) = \frac{1}{|\overrightarrow{S}|} \sum_{\overrightarrow{S_i} \in \overrightarrow{S}} RMSE(\overrightarrow{SM_i}, \overrightarrow{S_i}) \tag{9}$$

$$RMSE(\overrightarrow{SM_i}, \overrightarrow{S_i}) = \sqrt{\frac{1}{|\overrightarrow{S_i}|} \sum_{t \in \overrightarrow{S_i}} (log(S_{i,t}) - log(SM_{i,t}))^2} \tag{10}$$

$\overrightarrow{SM_i}$ are the soil-moisture time series of a specific probe/position i, respectively, from real probes and the simulator. Consistently, $S_{i,t}$ and $SM_{i,t}$ represent the soil moisture values at a time t. Finally, $error()$ averages the $RMSE()$ over all the sensors/positions. Soil moisture (i.e., $S_{i,t}$ and $SM_{i,t}$) ranges over several degrees of magnitude, thus the same nominal variation may have a different significance (e.g., a variation of 50 cbar in the range of $[0, -100]$ cbar has a higher impact than in $[-100, -1000]$ cbar). By computing the logarithm we make variations comparable and their average meaningful.

Algorithm 2 initializes the history of explored configurations (Line 1) and the number of iterations (Line 2). While the iteration budget is not exhausted (Line 3), we increase the iterations (Line 4), optimize the tunable parameters through Bayesian Optimization (Line 5), forecast the soil moisture trend with Orchard3D-Lab (Line 6), compute the approximation error (Line 7), and add the explored configuration along with its error to the history (Line 8). Finally, when the budget is exhausted, the best configuration is returned (Line 9). We recall that $BayesianOpt()$ carries out a smart exploration of the parameter search space that finds out good configuration even with a limited budget.

To the best of our knowledge, Orchard3D-Lab is the only hydrology process-based model that leverages this innovative family of optimization methods. Other tools (e.g., HYDRUS) employed either local (e.g., the Marquardt–Levenberg algorithm) or model-free (e.g., genetic algorithms) optimization methods.

3. Material and methods

The system has been tested on a kiwi orchard in the hills of central-northern Italy, part of a commercial farm that was selected to represent the real conditions for kiwi production in the area. We verify how accurately the system, properly tuned, can simulate the real soil behavior. The tests refer to the period June-August 2022 for which weather forecasts, planned irrigation, and real soil moisture (our ground truth) time series were collected.

3.1. System parameters

The total length of the field is 170 m, the inter-row distance (plant to plant) is 4.5 m, and the intra-row distance is 2 m. Table 2 reports the system parameters for the simulated plant.

The orchard is located in Errano (Faenza, Emilia-Romagna, Italy), having a latitude of 44.28, a longitude of 11.92, and an altitude of 62 m. The slopes were set based on field measurements performed with a total station, specifically: $-1\ \mathrm{m} \cdot \mathrm{m}^{-1}$ horizontally and $2.5\ \mathrm{m} \cdot \mathrm{m}^{-1}$ vertically. From the center of the intra-row, a 1 m long mound with $20\ \mathrm{m} \cdot \mathrm{m}^{-1}$ of slope extends in both directions. No water table was observed.

Basic soil properties were measured at the site, a single layer of 0.9 m with a loamy texture (30% sand, 30% silt, and 40% clay) based on the International Soil Science Society (ISSS) classification system. Soil water retention parameters were obtained from the parameter tuning procedure (a saturation threshold of $0.5\ L^3 \cdot L^{-3}$, a residual of $0.03\ L^3 \cdot L^{-3}$, and the related Van Genuchten parameters).

According to the orchard layout, for the simulated plant we considered three drippers in a single line (0.66 m apart from each other). The root system has been estimated to have a radius of 1.6 m and a depth of 0.8 m. According to Section 2.1.3, roots are taproot shaped; the $root_x$ and $root_z$ determine the shape shown in Fig. 3. The volume of the simulated parallelepiped is 2 m·2 m·0.8 m (the product of length, width, and depth). This allows to properly simulate the whole root system. The domain is discretized with a dynamic cell size: both length and width are set to 0.125 m, and depth ranges from 0.01 m to 0.04 m. Specifically, a geometrical progression was chosen in the first 0.2 m of soil.

3.2. Weather, watering, and soil moisture time series

All data were sampled hourly. Weather and watering variables were collected at the site through a weather station and a water meter, respectively. The 1-, 3-, and 7-day weather forecasts, to be provided to the model as simulation inputs, were provided by the weather regional service ARPAE (Environmental Prevention Agency, 2024). We monitored the field from May to October 2022 and selected the period of the actual irrigation season: from June 21st to August 31st. Fig. 7 depicts the trend of air humidity, air temperature, solar radiation, and wind speed through the whole period. In general, air humidity and temperature show a hot and damp summer, with a peak of 39 °C of air temperature and 97.7% humidity. The period was poorly ventilated, and solar radiation is typical of the area with values ranging from about 350 in March to 750 W m^{-2} in July. The water balance in

Table 2
System parameters values for our case study.

Type	Parameter	Value
Field	Location	Latitude = 44.28, Longitude = 11.92, Altitude = 62 m
	Slopes	Horizontal = -0.01 m · m^{-1}, Vertical = -0.025 m · m^{-1}
	Mound	Slope = 0.2 m · m^{-1}, width = 1 m
	Water table	None
Soil Layer[a]	Thickness	0.9 m
	Texture	Sand = 30%, Silt = 30%, Clay = 40%
	Ksat	$1.1 \cdot 10^{-6}$
	θ_s	0.5 m^3 · m^{-3}
	θ_r	0.03 m^3 · m^{-3}
	α	1.9 m^{-1}
	n	1.5
	he	0.23 m H_2O
	b	None
Plant[a]	Position	First = (0.0, −0.3)
	Radius	1.6 m
	Leaf area index	4.5
	Root depth	0.8 m
	Root deformations	$root_x = 0.0$, $root_z = 0.8$
	Kc max	2.6
	fRAW	0.5
Irrigation elem[a]	Type	Single-line Dripper
	Position	First = (0.0, −0.67), Second = (0.0, 0.0), Third = (0.0, 0.67)
Model	Geometry	Length = 2 m, Width = 2 m, Depth = 0.8 m
	Cell size	min = 0.01 m, max = 0.04 m
	Retention curve	mod. Van Genuchten
	Conductivity mean	log
	Conductivity H/V Ratio	1.0

Parameters in bold are targeted by the parameter tuning.
[a] Types can have several elements.

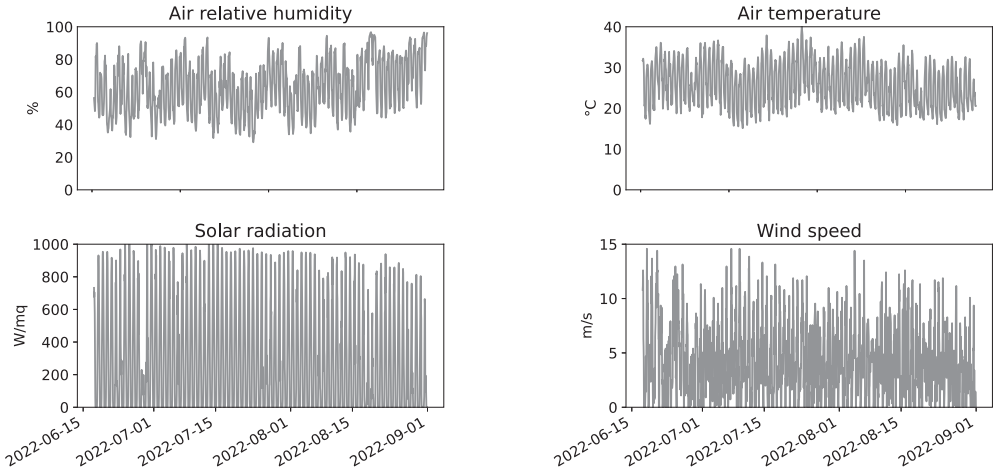

Fig. 7. Weather time series throughout the simulation period.

Fig. 8 provides a detailed description of the water dynamics of the orchard. We observed an extremely dry season w.r.t. precipitation; the only significant rain was detected around mid-August. Hence, the drainage is present only after the rains of August and a constant amount of irrigation was mandatory in the remainder extent of time. The evaporation is always contained, below or around 1 mm · d^{-1} (which corresponds to one liter per square meter) due to the kiwi leaf cover which shades the ground. On the other hand, the transpiration demand is very high, some days even over 10 mm · d^{-1}, but irrigation amounts and schedule are adequate for the demand—apart from the excessive irrigation of 20 mm in June. Therefore, the plant never experienced water stress, as can be seen from the fact that the actual transpiration is always equal to or close to the maximum required by the weather conditions.

As to the soil moisture of the monitored tree, we installed a 2D probe grid of 12 GB-1 Gypsum Block Sensors[2] (Delmhorst Inc.) as shown in Fig. 1. The grid was orthogonal to the y axis (i.e., the intra-row line), with 0.2 m of translation from the plant, with the top left corner under the dripper. As shown in Fig. 9, probes were organized on three different depths (0.2 m, 0.4 m, 0.6 m on the z axis), with four elements per level on the x axis ($\approx$ 0.25 m to each other). Probe values are collected through a LoRaWan network every 15 min.

[2] A Gypsum Block Sensor consists of two electrodes mounted in a small block of porous material: as the soil dries out water is extracted from the gypsum block and the resistance reading between the electrodes increases. When the soil is wetted, water is drawn back into the block and the resistance decreases.

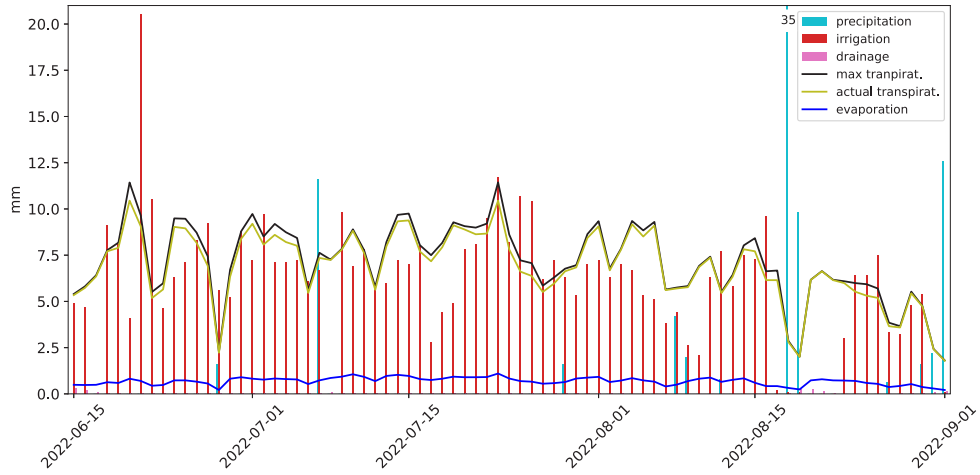

Fig. 8. Water balance throughout the period.

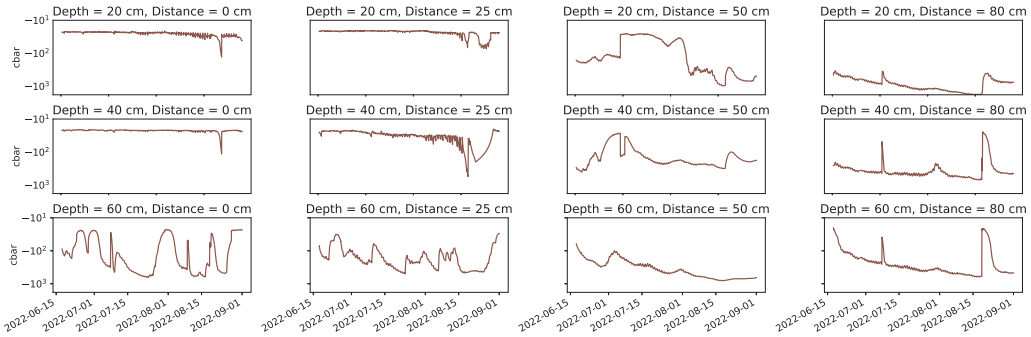

Fig. 9. Water potential time series of the 12 probes throughout the simulation period.

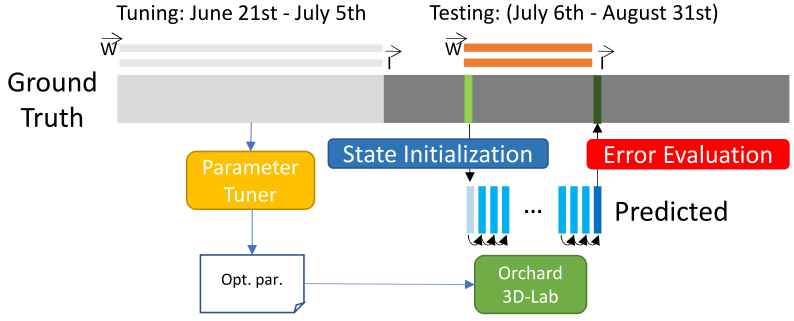

Fig. 10. The evaluation methodology.

3.3. Evaluation methods

Tests involve both Orchard3D-Lab and the Parameter Tuner modules. All the tests are run on an Intel Core i7 machine running at 3.20 GHz with 64 GB of main memory.

As to the efficiency of the online phase, we collected the average forecasting execution time for Orchard3D-Lab. As to effectiveness, tests are aimed at verifying the simulation accuracy and comparing it with a standard baseline to better understand the improvement. We adopted the following testing methodology (see Fig. 10):

- The available dataset has been split in two: the first two-week period (June 21st–July 5th) is used for tuning the parameters, while the remaining samples (July 6th–August 31st) were exploited for testing.
- Parameter Tuner is fed with ground truth weather data collected at the site.
- We tested Orchard3D-Lab with three different forecasting horizons: 1, 3, and 7 days ahead.
- For every timestamp t in the testing period, we run the state initialization procedure (see Section 2.2) to compute the initial state SM_{Init} and then we fed Orchard3D-Lab providing with $\overrightarrow{W}$ and $\overrightarrow{I}$ according to the forecasting horizon. $\overrightarrow{W}$ are the weather conditions forecasted at time t by the weather regional service ARPAE (Environmental Prevention Agency, 2024). Irrigation data

$\vec{I}$ is instead a known input (the farmer/system decides when to water).

For instance, given a horizon of 3 days, Orchard3D-Lab (i) initializes the soil moisture state with the first sample, (ii) iterates the simulation for the duration of 72 samples using as input the output of the previous iteration, and (iii) calculates the error between observed and final simulated samplings.

The Parameter Tuner is the data-driven process that automatically determines the right parameters for the current use case. The tuner should retain its effectiveness even when a reduced amount of examples is available, resulting in a shorter sampling period to tune Orchard3D-Lab. To verify the Parameter Tuner robustness we progressively reduce the tuning period (75%, 50%, and 25% of June 21st–July 5th) and evaluate the performance of the returned sets of parameters (Fig. 10).

4. Results

4.1. Orchard3D-Lab efficiency

The computation time needed for forecasting soil moisture in a future state depends on the current water content of the soil and the amount of irrigation/precipitation of each hour (the more the watering, the more expensive the calculation). Throughout the whole period, we observed an average of 2 s in forecasting the soil moisture of the next hour, 48 s for a 1-day horizon, 144 s (≈ 2 min) for a 3-day horizon, and 336 s (≈ 5 min) for a 7-day horizon.

4.2. Orchard3D-Lab effectiveness

Figs. 11 and 12 show a graphical representation of the measured soil moisture profile and compare it with the forecasting results. Colors emphasize water potential values according to five crop-specific soil moisture ranges (suggested by agronomist during the Agro.Big.Data.Science project (The Agro.Big.Data.Science Project, 2020)): dark blue (in $[0, -30)$ cbar) and light blue (in $[-30, -100)$ cbar) show heavily/slightly portions of over-watered soil, salmon pink (in $[-100, -300)$ cbar) represents the ideal case (Miller et al., 1998), while light red (in $[-300, -1500)$ cbar) and dark red (in the range of $[-1500, -10000)$ cbar) show portions of slightly/heavily under-watered soil. Note that, as water potential is not linear, the ranges of values are smaller when the water potential is closer to the field capacity (i.e., the soil is more saturated). Consequently, forecasting errors must be smaller when the water potential is closer to 0 (i.e., very wet soil).

While Fig. 11 shows the soil moisture trend along the overall testing period, Fig. 12 spatially details the profile at 10 am on July 26th. The fine-grained spatial grid clearly shows how moisture changes depending on the dripper distance and according to the effect of the root system. Forecasted profiles (sub-figures (b), (c), and (d)) are very similar to the observed ones with slight differences appearing as the forecasting horizon increases.

Fig. 13 is a numerical representation of Fig. 11. It reports the average water potentials of the sensor grid over time, as defined in Eq. (11), where $\overrightarrow{X_t}$ can be substituted by $\overrightarrow{S_t}$ and $\overrightarrow{SM_t}$ at different time horizons.

$$AvgPotential(\overrightarrow{X_t}) = \frac{1}{|\overrightarrow{X_t}|} \sum_{\overrightarrow{X_{i,t}} \in \overrightarrow{X_t}} \overrightarrow{X_{i,t}} \tag{11}$$

Given the very dry season and the heavy rainfall in those days, the soil presented unexpected macropores and cracks in the sub-surface layers. This resulted in a non-uniform distribution and unexpected changes in the soil moisture dynamics, which the model was unable to fully capture due to its limitation in accounting for preferential flows. Yet, it is worth noticing how the state initialization mechanism allows Orchard3D-Lab to recognize such events, reset to the actual state, and quickly reduce the error. Forecasts with shorter horizons reinitialize earlier and react faster to changes.

Table 3
Forecasting error (Eq. (9)) considering different portions of tuning data.

Percentage of tuning period	Forecasting horizon		
	1 day	3 days	7 days
25%	0.43	0.69	0.79
50%	0.40	0.63	0.79
75%	0.40	0.63	0.83
100%	0.38	0.59	0.73

Finally, Fig. 14 reports a scatterplot showing the correlation between observed and forecasted water content. The regression lines show the overall trend. The closer the forecasted values are to the observed ones, the lower the regression line diverges from the chart diagonal (i.e., from the full correlation between the two variables). Variables are well correlated on all time horizons with the best performance being 1-day forecast. Orchard3D-Lab tends to estimate the soil slightly over-moistured for high values of water content but is extremely accurate for low values.

4.3. Parameter tuning effectiveness

Table 3 shows that errors slightly decrease when more tuning data are available for every forecasting horizon. More data translates into more hydraulic dynamic examples, which are useful to better estimate the parameters, and hence make the forecasts more reliable. Although the general trend, Orchard3D-Lab achieves good performance even with 25% and 50% of the considered period. Above all, the case of 50% does not consider the rain at the beginning of June (which brings some fluctuations in the calculus) and achieves excellent performance. The standard deviation remains steady along the forecasting horizon. Overall, the insights suggest that the tuning phase of Orchard3D-Lab is robust in suggesting soil and plant parameters for the use case at hand.

5. Discussion

An irrigation forecasting system for precision agriculture is effective if its accuracy enables an effective watering policy. According to the agronomy researchers involved in the Agro.Big.Data.Science (The Agro.Big.Data.Science Project, 2020), relative errors up to 50% between the predicted and the actual values are permissible because they do not impact watering choices. For example, reminding that water potential is not linear, predicting a moisture value of −300 cbar when the actual moisture is −200 cbar does not invalidate the agronomist evaluation; the same happens if the predicted moisture value is −3000 cbar when the actual moisture is −2000 cbar. Fig. 15 reports the relative error along time computed as:

$$RelErr(\overrightarrow{S_t}, \overrightarrow{SM_t}) = \frac{AvgPotential(\overrightarrow{S_t}) - AvgPotential(\overrightarrow{SM_t})}{AvgPotential(\overrightarrow{S_t})} \tag{12}$$

the three lines shows simulations, $\overrightarrow{SM}$, computed using different forecasting horizons. Orchard3D-Lab was able to remain well below the 50% relative error threshold during the whole season below 25% of relative error for the 93%, 87%, and 86% of the season for respectively (1-, 3-, and 7-day horizons), with an exception occurred around mid-August after heavy rain.

To better appreciate Orchard3D-Lab performance, we compared it with a Persistent System forecaster (i.e., the forecasted water potential is the current one) that we use as a baseline. reports the average prediction RMSE (see Eq. (10)) through the whole period. Orchard3D-Lab outperforms the baseline for 3 out of 4 forecasting horizons. It should be noted that a Persistent System has an advantage when tests are carried out on an orchard which, as a matter of cultivation policy, is watered every day to maintain water potential constant. Limited variations in water potential (due to constant daily irrigation) favor

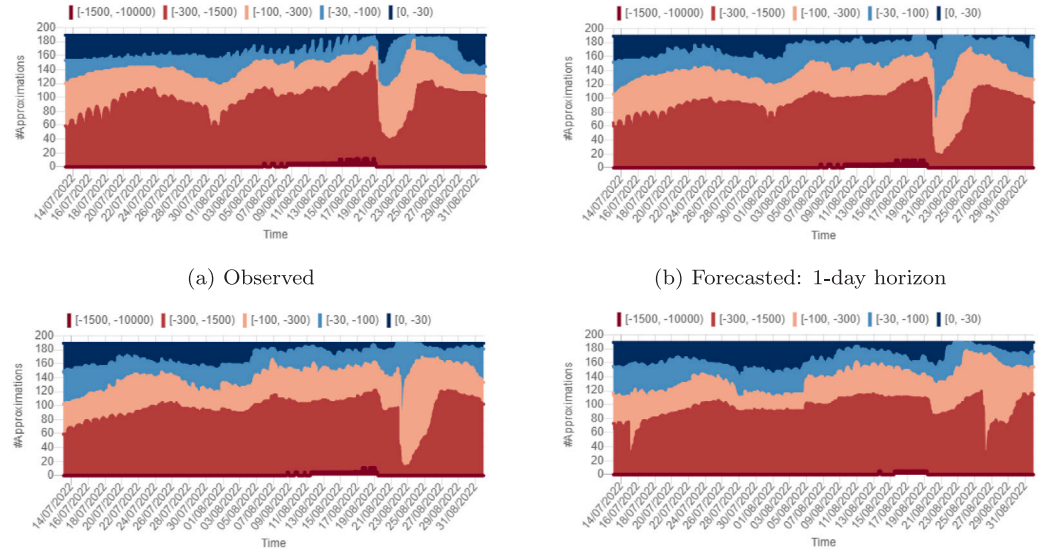

(a) Observed (b) Forecasted: 1-day horizon

(c) Forecasted: 3-days horizon (d) Forecasted: 7-days horizon

Fig. 11. Soil moisture trend over the period.

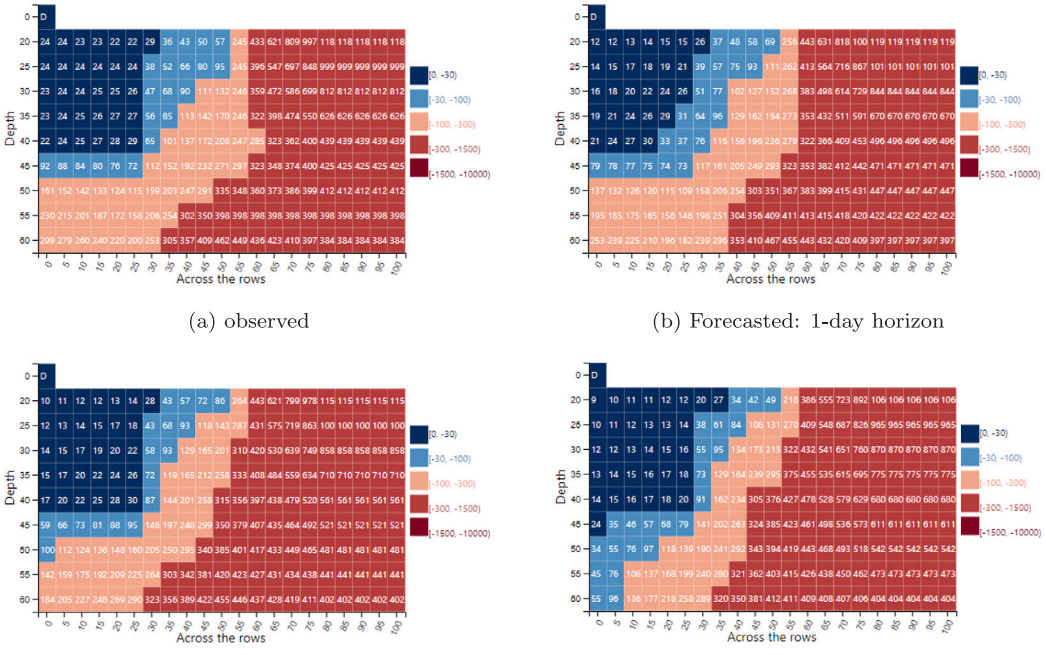

(a) observed (b) Forecasted: 1-day horizon

(c) Forecasted: 3-days horizon (d) Forecasted: 7-days horizon

Fig. 12. 2D-spatial soil moisture profiles.

Table 4
Comparison of the RMSE (Eq. (10)) for Orchard3D-Lab and the Persistent System considering different irrigation policies and forecasting horizon.

Orchard3D-Lab \ Persistent System		Forecasting horizon 1 day		Forecasting horizon 3 days		Forecasting horizon 7 days	
Irrigation policy	(2022) Daily	**0.38**	0.44	**0.59**	0.61	0.73	**0.72**
	(2024) Weekly	**0.36**	0.54	**0.56**	0.70	**0.57**	0.71

the Persistent System, which will have a smaller error although the Persistent System is unaware of irrigation (i.e., the forecasted value is independent of values in $\vec{I}$). For this reason, we also use data collected in 2024 when, for research purposes, a weekly irrigation policy was used; this results in a sensitive fluctuation of soil moisture and irrigation over time.

Orchard3D-Lab largely outperforms the Persistent System when a weekly irrigation policy is adopted. The average error is 0.36 for the 1-day horizon, 0.56 for the 3-day horizon, and 0.57 for the 7-day horizon.

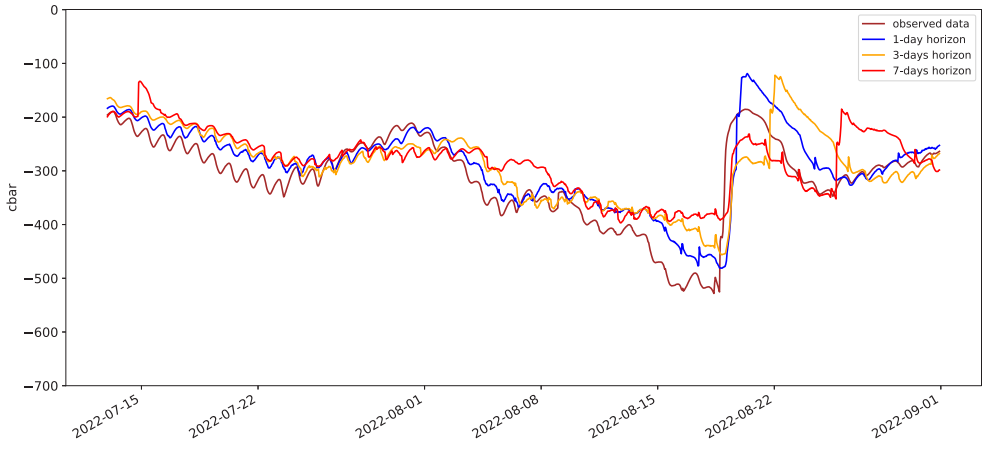

Fig. 13. Averaged (observed) water potential $\overline{S}$ and Orchard3D-Lab simulations $\overline{SM}$ according to the forecasting horizons.

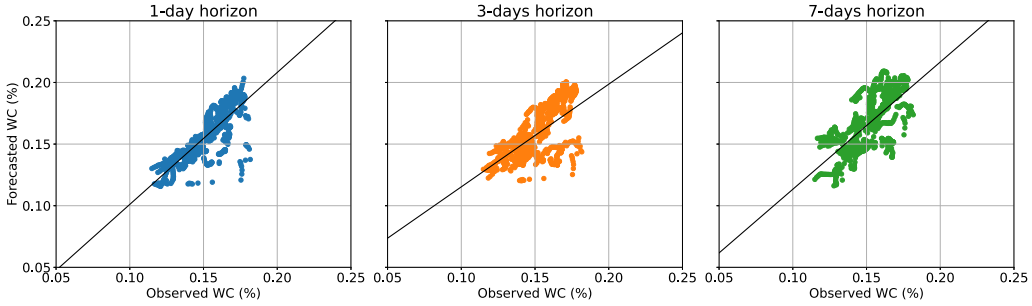

Fig. 14. Correlation between observed and forecasted water content (%).

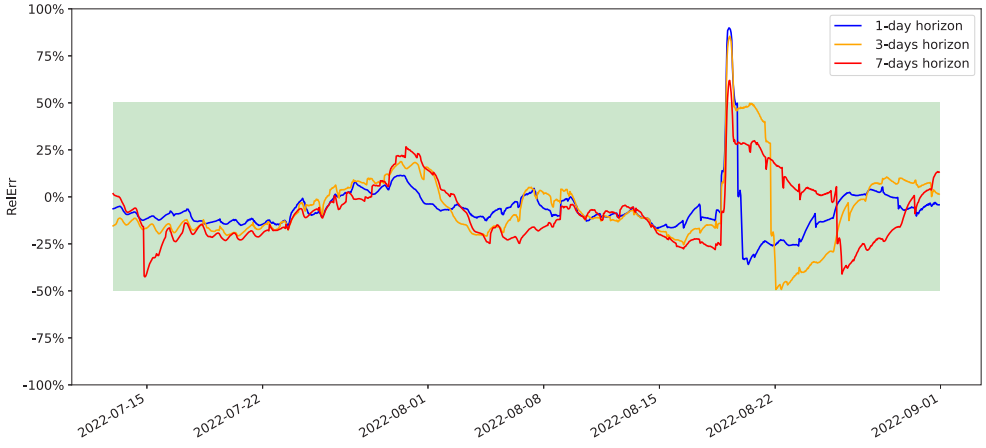

Fig. 15. Water potential relative errors. The green region defines the relative error limit for which the forecast is considered reliable.

The advanced prediction model of Orchard3D-Lab makes it more useful as the forecasting horizon increases. This makes it particularly suitable in the most critical contexts, e.g. those in which daily irrigation is not possible due to water resource scarcity or business constraints. In these cases, an accurate prediction of soil moisture evolution is fundamental to provide the soil with the correct amount of water to minimize hydric stress throughout the forecast horizon.

6. Conclusions

We presented an integrated system coupling a three-dimensional process-based model with a state initialization procedure that exploits a two-dimensional probe grid. Forecasted soil moisture data up to a 7-day horizon has proven to be precise enough to support precision watering. Testing has been carried out on a real Kiwifruit orchard. Data from real probes are also used to auto-tune the soil parameters to achieve effective field-specific forecasts. Robustness tests emphasized that a few days of hourly samples are enough to properly set the field parameters, making our approach practically applicable.

We are now working towards creating a prescriptive system delivering watering advice. Orchard3D-Lab will be exploited to forecast the combined effects of weather conditions and watering policies. Coupling Orchard3D-Lab with an optimizer allows the testing of different policies

and computing the watering advice that best fits an optimal soil moisture profile. Working on a 7-day period, we can handle complex cases where constraints (e.g., water availability) do not allow daily irrigation.

CRediT authorship contribution statement

Marco Bittelli: Writing – original draft, Formal analysis, Conceptualization. **Matteo Francia:** Writing – review & editing, Software, Conceptualization. **Joseph Giovanelli:** Writing – original draft, Software. **Matteo Golfarelli:** Writing – review & editing, Supervision, Formal analysis, Conceptualization. **Fausto Tomei:** Validation, Software, Formal analysis, Conceptualization.

Acknowledgments

This study was carried out within the Agritech National Research Center and received funding from the European Union Next-GenerationEU (PIANO NAZIONALE DI RIPRESA E RESILIENZA (PNRR) - Mission 4 Component 2, Investment 1.4 - D.D. 1032 17/06/2022, CN00000022). This manuscript reflects only the authors' views and opinions, neither the European Union nor the European Commission can be considered responsible for them.

Software and data availability

The source code and all data (both input and output) are available on the GitHub repository at https://github.com/big-unibo/orchard3d-lab. A demo of Orchard3D-Lab is available at https://big.csr.unibo.it/projects/orchard3d-lab.

References

Allen, R.G., Pereira, L.S., Raes, D., Smith, M., et al., 1998. Crop evapotranspiration-guidelines for computing crop water requirements-FAO Irrigation and drainage paper 56. 300, D05109, (9).

Baldi, E., Francia, M., Gallinucci, E., Giovanelli, J., Golfarelli, M., Quartieri, M., Toselli, M., 2023. Method and system for soil-moisture monitoring. IT Patent 102021000023162.

Bittelli, M., 2010. Measuring soil water potential for water management in agriculture: A review. Sustainability 2 (5), 1226–1251. http://dx.doi.org/10.3390/su2051226.

Bittelli, M., Campbell, G.S., Tomei, F., 2015. Soil Physics with Python. Oxford University Press, Oxford, UK, http://dx.doi.org/10.1093/acprof:oso/9780199683093.001.0001.

Driessen, P.M., Konijn, N.T., 1992. Land-use systems analysis. WAU and Interdisciplinary Research (INRES).

2024. Environmental prevention agency and energy Emilia-Romagna (ARPAE). URL https://dati.arpae.it/.

Francia, M., Giovanelli, J., Golfarelli, M., 2022. Multi-sensor profiling for precision soil-moisture monitoring. Comput. Electron. Agric. 197, 106924. http://dx.doi.org/10.1016/j.compag.2022.106924.

Frazier, P.I., 2018. A tutorial on Bayesian optimization. CoRR abs/1807.02811 arXiv:1807.02811 URL http://arxiv.org/abs/1807.02811.

Grisafi, F., DeJong, T.M., Tombesi, S., 2022. Fruit tree crop models: an update. Tree Physiol. 42 (3), 441–457.

Honari, M., Ashrafzadeh, A., Khaledian, M., Vazifedoust, M., Mailhol, J., 2017. Comparison of HYDRUS-3D soil moisture simulations of subsurface drip irrigation with experimental observations in the south of France. J. Irrig. Drain. Eng. 143 (7), 04017014. http://dx.doi.org/10.1061/(asce)ir.1943-4774.0001188.

Ippisch, O., Vogel, H.-J., Bastian, P., 2006. Validity limits for the van Genuchten–Mualem model and implications for parameter estimation and numerical simulation. Adv. Water Resour. 29 (12), 1780–1789. http://dx.doi.org/10.1016/j.advwatres.2005.12.011.

Judd, M., McAneney, K., Trought, M., 1986. Water use by sheltered kiwifruit under advective conditions. N. Z. J. Agric. Res. 29 (1), 83–92. http://dx.doi.org/10.1080/00288233.1986.10417978.

Keating, B.A., Carberry, P.S., Hammer, G.L., Probert, M.E., Robertson, M.J., Holzworth, D., Huth, N.I., Hargreaves, J.N., Meinke, H., Hochman, Z., et al., 2003. An overview of APSIM, a model designed for farming systems simulation. Eur. J. Agron. 18 (3), 267–288. http://dx.doi.org/10.1016/s1161-0301(02)00108-9.

Luo, G., Stone, B.L., Johnson, M.D., Tarczy-Hornoch, P., Wilcox, A.B., Mooney, S.D., Sheng, X., Haug, P.J., Nkoy, F.L., et al., 2017. Automating construction of machine learning models with clinical big data: Proposal rationale and methods. JMIR Res. Protoc. 6 (8), e175. http://dx.doi.org/10.2196/resprot.7757.

Lv, T., Wang, L., Xie, H., Zhang, X., Zhang, Y., 2021. Evolutionary overview of water resource management (1990–2019) based on a bibliometric analysis in Web of Science. Ecol. Inform. 61, 101218. http://dx.doi.org/10.1016/j.ecoinf.2021.101218.

Marshall, T.J., Holmes, J.W., Rose, C.W., 1996. Soil Physics. Cambridge University Press, http://dx.doi.org/10.1017/cbo9781139170673.

Miller, S., Smith, G., Boldingh, H., Johansson, A., 1998. Effects of water stress on fruit quality attributes of kiwifruit. Ann. Botany 81 (1), 73–81. http://dx.doi.org/10.1006/anbo.1997.0537.

Morianou, G., Kourgialas, N.N., Karatzas, G.P., 2023. A review of HYDRUS 2D/3D applications for simulations of water dynamics, root uptake and solute transport in tree crops under drip irrigation. Water 15 (4), 741. http://dx.doi.org/10.3390/w15040741.

Nagahage, E.A.A.D., Nagahage, I.S.P., Fujino, T., 2019. Calibration and validation of a low-cost capacitive moisture sensor to integrate the automated soil moisture monitoring system. Agriculture 9 (7), 141. http://dx.doi.org/10.3390/agriculture9070141.

Rallo, G., Paço, T., Paredes, P., Puig-Sirera, À., Massai, R., Provenzano, G., Pereira, L., 2021. Updated single and dual crop coefficients for tree and vine fruit crops. Agricult. Water. Manag. 250, 106645. http://dx.doi.org/10.1016/j.agwat.2020.106645.

Richards, L.A., 1931. Capillary conduction of liquids through porous mediums. Physics 1 (5), 318–333. http://dx.doi.org/10.1063/1.1745010.

Sau, F., Boote, K.J., McNair Bostick, W., Jones, J.W., Inés Mínguez, M., 2004. Testing and improving evapotranspiration and soil water balance of the DSSAT crop models. Agron. J. 96 (5), 1243–1257. http://dx.doi.org/10.2134/agronj2004.1243.

Serrano-Notivoli, R., Longares, L.A., Cámara, R., 2022. Bioclim: An R package for bioclimatic classifications via adaptive water balance. Ecol. Inform. 71, 101810. http://dx.doi.org/10.1016/j.ecoinf.2022.101810.

Silva, J.V., Giller, K.E., 2020. Grand challenges for the 21st century: what crop models can and can't (yet) do. J. Agric. Sci. 158 (10), 794–805. http://dx.doi.org/10.1017/s0021859621000150.

Silva, R., Paço, T., Ferreira, M., Oliveira, M., 2008. Transpiration of a kiwifruit orchard estimated using the granier sap flow method calibrated under field conditions. In: V International Symposium on Irrigation of Horticultural Crops 792. Vol. 792, International Society for Horticultural Science, pp. 593–600. http://dx.doi.org/10.17660/actahortic.2008.792.70.

2020. The agro.big.data.science project. http://agrobigdatascience.it/. (Last Accessed 18 October 2021).

Villani, G., Tomei, F., Tomozeiu, R., Marletto, V., 2011. Climatic scenarios and their impacts on irrigated agriculture in Emilia-Romagna, Italy. Ital. J. Agrometeorol. 16 (1).

Vitali, G., Francia, M., Golfarelli, M., Canavari, M., 2021. Crop management with the IoT: An interdisciplinary survey. Agronomy 11 (1), 181. http://dx.doi.org/10.3390/agronomy11010181.

Wang, C., Wu, Q., Weimer, M., Zhu, E., 2021. FLAML: A fast and lightweight automl library. In: Smola, A., Dimakis, A., Stoica, I. (Eds.), Proceedings of Machine Learning and Systems 2021, MLSys 2021, Virtual, April 5-9, 2021. mlsys.org, pp. 434–447, URL https://proceedings.mlsys.org/paper/2021/hash/92cc227532d17e56e07902b254dfad10-Abstract.html.

Ye, L., Cai, Q., Zhang, M., Tan, L., 2014. Real-time observation, early warning and forecasting phytoplankton blooms by integrating in situ automated online sondes and hybrid evolutionary algorithms. Ecol. Inform. 22, 44–51. http://dx.doi.org/10.1016/j.ecoinf.2014.04.001.